Redistribution of metabolic resources through astrocyte networks mitigates neurodegenerative stress

Melissa L. Cooper[a], Silvia Pasini[a], Wendi S. Lambert[a], Karis B. D'Alessandro[a], Vincent Yao[a], Michael L. Risner[a], and David J. Calkins[a,1]

[a]Department of Ophthalmology and Visual Sciences, Vanderbilt University Medical Center, Nashville TN 37232-0654

Edited by Jeremy Nathans, The Johns Hopkins University School of Medicine, Baltimore, MD, and approved June 28, 2020 (received for review May 11, 2020)

In the central nervous system, glycogen-derived bioenergetic resources in astrocytes help promote tissue survival in response to focal neuronal stress. However, our understanding of the extent to which these resources are mobilized and utilized during neurodegeneration, especially in nearby regions that are not actively degenerating, remains incomplete. Here we modeled neurodegeneration in glaucoma, the world's leading cause of irreversible blindness, and measured how metabolites mobilize through astrocyte gap junctions composed of connexin 43 (Cx43). We elevated intraocular pressure in one eye and determined how astrocyte-derived metabolites in the contralateral optic projection responded. Remarkably, astrocyte networks expand and redistribute metabolites along distances even 10 mm in length, donating resources from the unstressed to the stressed projection in response to intraocular pressure elevation. While resource donation improves axon function and visual acuity in the directly stressed region, it renders the donating tissue susceptible to bioenergetic, structural, and physiological degradation. Intriguingly, when both projections are stressed in a WT animal, axon function and visual acuity equilibrate between the two projections even when each projection is stressed for a different length of time. This equilibration does not occur when Cx43 is not present. Thus, Cx43-mediated astrocyte metabolic networks serve as an endogenous mechanism used to mitigate bioenergetic stress and distribute the impact of neurodegenerative disease processes. Redistribution ultimately renders the donating optic nerve vulnerable to further metabolic stress, which could explain why local neurodegeneration does not remain confined, but eventually impacts healthy regions of the brain more broadly.

astrocyte | neurodegeneration | astrocyte network | gap junction | metabolism

The brain accounts for 30 to 50% of our resting rate of energy consumption, despite comprising only 2% of human body mass (1–3). Neurons rely primarily on glucose as a substrate for ATP production, which depletes quickly during periods of high demand or stress (4–6). In the central nervous system, neuronal energy needs are satisfied through interactions with astrocyte glia, which create and store glycogen as a safeguard against periods of stress (4, 7–11). This metabolic collaboration between neurons and astrocytes is critical to tissue survival during injury, such as in ischemia, and in neurodegenerative disease, such as during Alzheimer's, Parkinson's, and Huntington's diseases, among many others (7, 12, 13). Such conditions tax normal energy utilization through increased oxidative stress and diminished metabolic capacity (7, 14, 15).

Like other age-related neurodegenerations, glaucomatous optic neuropathy (or glaucoma) involves astrocyte remodeling during insult, in this case to the axons of retinal ganglion cell neurons that form the optic projection to the brain (16). These axons include a lengthy unmyelinated segment that traverses the retina that is especially vulnerable to metabolic and oxidative stress in glaucoma (17, 18). This stress arises from sensitivity to intraocular pressure (IOP) conveyed at the optic nerve head (19–21), which underlies glaucoma's stature as the world's leading cause of irreversible (i.e., neurological) blindness (22). Early progression involves axonal dysfunction, including degradation of anterograde transport to central projection sites in the brain and accumulation of phosphorylated neurofilaments linked to local depletion of mitochondria (15, 23, 24). These changes map closely to extensive redistribution of astrocyte processes in the optic nerve (23, 25–27). Astrocyte networks share cytoplasmic information via gap junctions comprised primarily of connexin 43 (Cx43) (28, 29), which is up-regulated in the glaucomatous optic nerve head (30). Since Cx43 is permeable to molecules up to 1 to 1.2 kDa (28, 31), we probed to what extent astrocyte gap junction-coupling mediates redistribution of much smaller energy substrates in response to neurodegenerative stress in the optic projection. We find that expanding Cx43-mediated networks of astrocytes redistribute metabolites over the exceptional distances between unstressed and stressed optic nerve projections from the two eyes. While preventing this distribution accelerates loss of neuronal function and degradation of visual acuity, redistribution renders donating tissue vulnerable to further metabolic stress. Thus, we posit that astrocyte networks utilize gap junctions through an endogenously protective mechanism that serves as a metabolic buffer against bioenergetic stress to distribute the impact of degenerative processes and preserve neuronal function.

Astrocyte CX43 Conditional Knockout Reduces Metabolite Transfer. To test the possibility that a transfer of astrocyte-derived

Significance

Astrocytes respond to neuronal energy needs by mobilizing metabolic stores. How these resources are mobilized during neurodegeneration, especially in nearby regions that are not actively degenerating, could impact new therapeutic approaches. We modeled neurodegeneration in glaucoma and measured how metabolites mobilize through astrocyte networks. We elevated pressure in one eye and determined how astrocyte-derived metabolites in the opposite eye and nerve responded. Remarkably, astrocyte networks expand and redistribute metabolites along distances nearly 1 cm in length to donate resources from unstressed to stressed tissue. While resource donation improves axon function and visual acuity, it renders the donating tissue susceptible to further stress, which could help explain why local neurodegeneration eventually impacts healthy regions of the brain.

Author contributions: M.L.C., S.P., and D.J.C. designed research; M.L.C., S.P., W.S.L., K.B.D., V.Y., and M.L.R. performed research; M.L.C. contributed new reagents/analytic tools; M.L.C. analyzed data; and M.L.C. and D.J.C. wrote the paper.

The authors declare no competing interest.

This article is a PNAS Direct Submission.

[1]To whom correspondence may be addressed. Email: david.j.calkins@vumc.org.

This article contains supporting information online at https://www.pnas.org/lookup/suppl/doi:10.1073/pnas.2009425117/-/DCSupplemental.

First published July 20, 2020.

resources occurs between healthy and degenerating tissue, we assessed the function of Cx43 in the optic nerve. We generated a mouse that allowed us to conditionally excise Cx43 from astrocytes under temporal and local control after mice reached 2 mo of age, 1 wk before any IOP elevation. We verified excision of the floxed portion of the *Cx43* gene in the retina, optic nerve, and cerebellum of *GFAP-Cre-ER^{T2}* × *Cx43$^{flox/flox}$* mice following tamoxifen gavage (knockout, KO) compared to gavage without tamoxifen (knockout control or KO-Ctrl) (Fig. 1 *A* and *B*). Induction successfully reduced label of Cx43 puncta by 98% across the retina, optic nerve, and superior colliculus (SC), the primary retinal projection site in the rodent brain (32, 33), when averaged between independent animals and tissues ($4.06 \times 10^5 \pm 1.28 \times 10^5$ puncta/mm^3 vs. $8.38 \times 10^3 \pm 6.65 \times 10^3$; $P < 0.001$) (Fig. 1*C*). In KO-Ctrl mice (without tamoxifen), Cx43 puncta distribute as expected along GFAP-labeled astrocyte processes and not in ganglion cells or their axons; tamoxifen treatment eradicated the majority of puncta (Fig. 1 *D*–*F*).

Using these mice, we next measured how conditional loss of Cx43 influences astrocyte glycogen in naïve optic nerve compared to nerves stressed by increasing periods of unilateral elevation in IOP and to their contralateral counterparts (Fig. 2*A*). Glycogen within the central nervous system is stored largely within astrocytes and represents the main reserve of metabolites for nervous tissues to utilize during periods of energetic deficit (34, 35). Glycogen stores diminish in the early stages of many

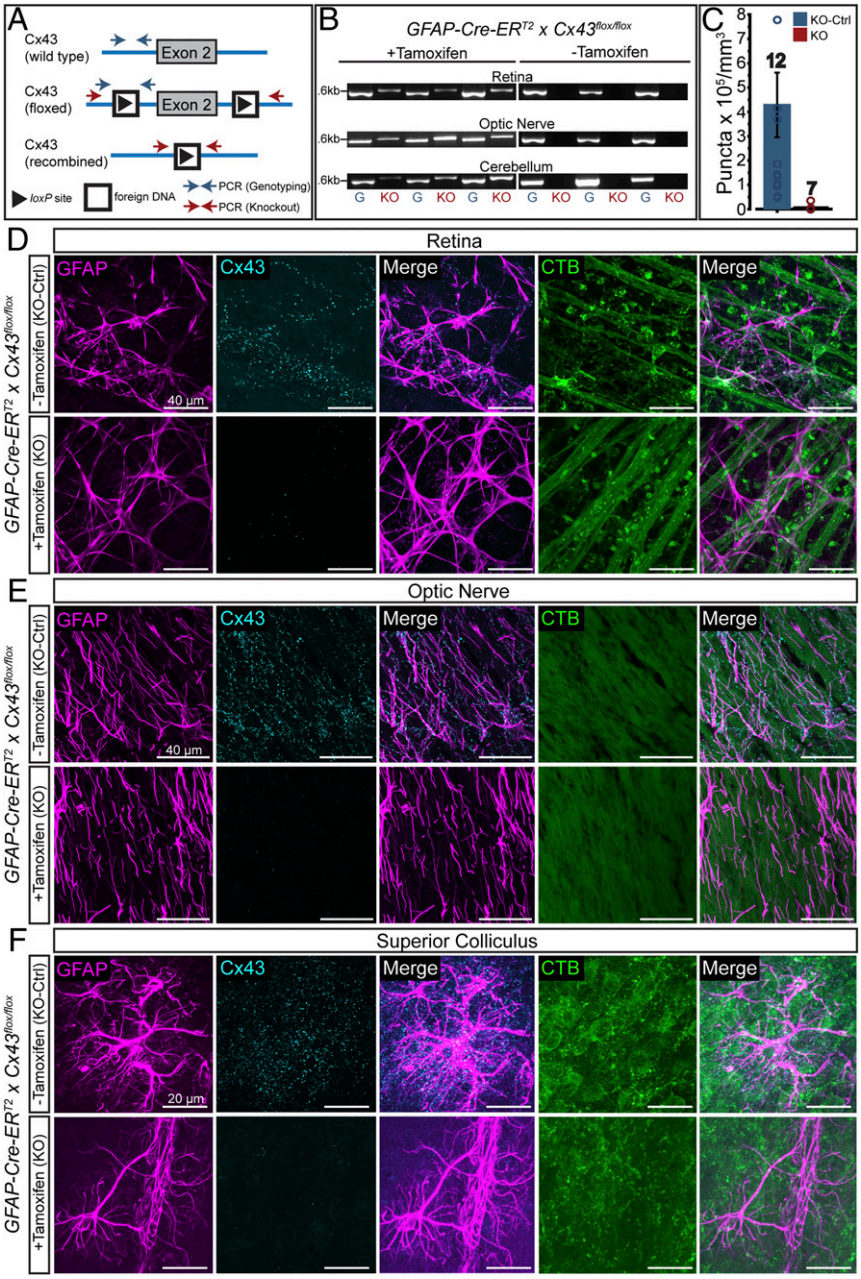

Fig. 1. Cx43 reduction in *GFAP-Cre-ER^{T2} x Cx43$^{flox/flox}$* mice. (*A*) Conditional mutagenesis of *Cx43$^{flox/flox}$* showing primers (arrows) for genotyping (blue) and verification of excision (red). (*B*) PCR products from nervous tissue in *Cx43$^{flox/flox}$* with genotype (G) and KO verification following induction. (*C*) Cx43$^+$ puncta/mm^3 decreased in KO retina, optic nerve, and SC compared to KO-Ctrl ($P < 0.001$; mouse numbers indicated). (*D*–*F*) KO reduces Cx43 immunolabel in GFAP-expressing astrocytes compared to KO-Ctrl. CTB labels retinal ganglion cells and their axon projections. (Scale bars, 40 µm in *D* and *E* and 20 µm in *F*.)

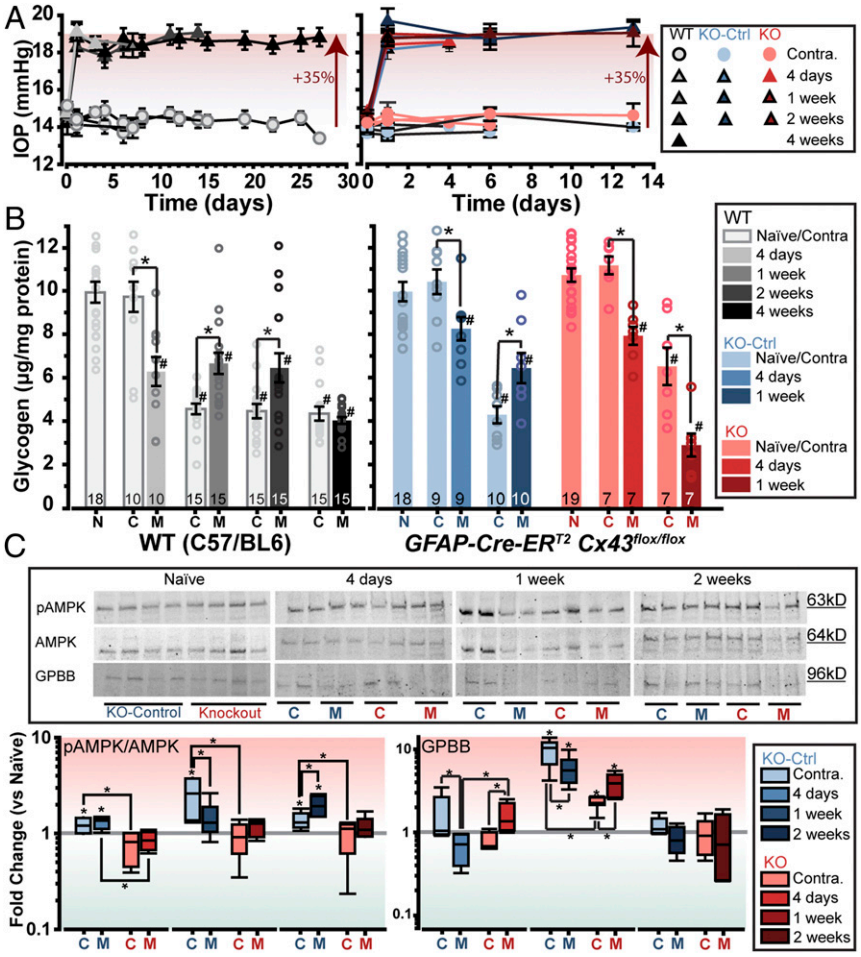

Fig. 2. Glycogen redistribution through astrocyte Cx43. (*A*) Elevated (Δ, +35%) vs. contralateral (C) IOP in WT (*Left*) and transgenic (*Right*) mouse eyes. (*B*) In WT mice (*Left*), microbead-elevated (M) IOP reduces glycogen vs. naïve (N) optic nerve ($^{\#}P \leq 0.005$). Glycogen diminishes with elevated IOP after 4 d but increases at 1 and 2 wk vs. contralateral (C, $^{*}P \leq 0.05$). For transgenic mice (*Right*), elevation decreases glycogen for both KO-Ctrl and KO vs. each respective naïve ($^{\#}P \leq 0.02$). In KO-Ctrl mice, glycogen decreases after 4 d elevation but increases after 1 wk vs. contralateral nerve ($^{*}P \leq 0.01$); for KO, glycogen decreases with both elevations vs. contralateral ($^{*}P < 0.001$). In KO-Ctrl, elevation increased glycogen compared to contralateral ($^{*}P = 0.04$), while in KO the opposite occurred ($^{*}P < 0.001$). (*C*) Western blots probing pAMPK, AMPK, and GPBB in naïve optic nerves (naïve GPBB Ctrl SEM ± 0.149, KO SEM ± 0.28; naïve pAMPK/AMPK Ctrl SEM ± 0.17, KO SEM ± 0.35) and in contralateral (C) vs. 4 d and 1- and 2-wk microbead (M) nerves (*Upper*). The pAMPK/AMPK ratio (*Lower Left*) increases in KO-Ctrl nerves (microbead and contralateral) vs. respective naïve ($n = 6$) for 4 d ($n = 5$) and 2 wk ($n = 5$) and in contralateral only at 1-wk ($n = 6$) microbead elevation ($^{*}P \leq 0.04$); ratio in KO nerves (M and C) does not change vs. respective naïve ($n = 6$, $P \geq 0.20$) and is less than ratio in KO-ctrl contralateral for all times ($n = 4$, $n = 7$, $n = 5$; $^{*}P \leq 0.01$). Ratio in KO-ctrl contralateral exceeds microbead at 1 wk ($^{*}P = 0.05$), while microbead exceeds contralateral at 2 wk ($^{*}P = 0.02$). Fold-change in GPBB (*Lower Right*) is increased at 4 d in KO-Ctrl contralateral vs. microbead nerves ($^{*}P = 0.04$) and in KO microbead vs. contralateral and vs. KO-Ctrl microbead nerves ($^{*}P \leq 0.03$). At 1 wk, GPBB increased vs. respective naïve in KO-Ctrl and KO nerves from both eyes ($^{*}P \leq 0.002$) and in KO-Ctrl contralateral vs. microbead and vs. KO contralateral ($^{*}P \leq 0.04$); GPBB increased more in KO microbead vs. contralateral ($^{*}P = 0.03$).

neurodegenerative diseases and insults that include metabolic stress (12, 36, 37). In the following experiments, we utilized the microbead occlusion model of glaucoma, a highly repeatable, widely utilized tool for IOP elevation (38). In this model, microbeads are injected into the anterior chamber of the eye where they impede aqueous fluid outflow, causing an increase in IOP of about 35%. This increase is similar to that of human patients with elevated IOP (39), causing gradual progression of neurodegeneration over the following 2 to 8 wk in rodents (16, 17).

In WT (C57/BL6) mice (Fig. 2 *B*, *Left*), 4 d of unilateral IOP elevation significantly diminished glycogen compared to both the optic nerve from naïve mice (−36.9%; $P < 0.001$) and the unstressed contralateral nerve from the same animal (−35.5%; $P < 0.001$). Glycogen did not differ significantly after 1 or 2 wk of elevation compared to 4 d ($P \geq 0.32$), although both exposures reduced glycogen compared to naïve mice (−33.1 and −35.1%, respectively; $P \leq 0.001$). Surprisingly, following 1 and 2 wk of IOP elevation, glycogen decreased even more dramatically in the unstressed contralateral optic nerve compared to the nerve stressed by IOP ($P < 0.001$, $P = 0.006$, respectively). The decrease was also significant compared to naïve mice (−54.3 and −56.4%, respectively; $P \leq 0.001$) and to nerves with 4 d of IOP elevation (−53.3 and 55.5%, respectively; $P \leq 0.001$). Four weeks of elevated IOP directly diminished optic nerve glycogen even further, compared to 1 wk (−36.0%, $P < 0.001$) and 2 wk (−39.7%, $P < 0.001$) of elevation and to naïve mice (−59.6%, $P < 0.001$). However, at this point glycogen in the contralateral nerve did not differ from that in the IOP-stressed nerve ($P = 0.202$), suggesting an equilibration.

We made subsequent measurements using IOP elevations of 4 d and 1 wk in KO and KO-Ctrl mice, as these times represent the period during which glycogen in the unstressed contralateral nerve most dramatically changed in the WT. As expected in KO-Ctrl

mice, 4 d of unilateral IOP elevation reduced glycogen compared to the unstressed contralateral nerve (−28.41%; $P = 0.01$); glycogen in each did not differ from their WT counterparts ($P = 0.233$ and $P = 0.466$, respectively) (Fig. 2 *B*, *Right*). As it did in WT nerves, glycogen diminished following 1 wk of IOP elevation in unstressed contralateral nerve compared to stressed for KO-Ctrl mice (−33.3%; $P = 0.012$). Following 4 d of IOP elevation, glycogen in KO nerves did not differ from KO-Ctrl ($P \geq 0.08$), once again decreasing in the IOP-stressed vs. the contralateral nerve (−30.9%, $P < 0.001$). However, 1 wk of IOP elevation in KO mice reversed the glycogen pattern observed in KO-Ctrl and WT mice. Although glycogen decreased in both IOP-stressed and contralateral KO nerves at 1 wk compared to 4 d of elevation (−63.4 and −43.1%, respectively; $P \leq 0.001$), the unstressed KO contralateral nerve contained significantly more glycogen than the IOP-stressed KO nerve (+55.6%; $P = 0.002$).

To assess metabolic state in the optic nerve, we measured via Western blots the ratio of pAMPK/AMPK, which increases with metabolic stress (40), and glycogen phosphorylase (GPBB) relative to total protein, which is a marker of glycogen breakdown (35). Only 32% of the mouse optic nerve is occupied by retinal ganglion cell axons, with the remainder representing glial cells (66%) and extracellular space (2%) (41), making the entirety of somatic protein as well as the majority of total protein within these samples glial in origin. In KO-Ctrl mice, nerves from unstressed contralateral eyes as well as nerves stressed by elevated IOP showed increased pAMPK/AMPK compared to naïve; KO of Cx43 eradicated this difference (Fig. 2 *C*, *Lower Left*). Furthermore, pAMPK/AMPK in KO-ctrl contralateral nerves consistently exceeded that in KO contralateral nerves ($^*P \leq 0.01$), demonstrating the necessity of astrocyte Cx43 for conveying metabolic stress due to elevated IOP. GPBB only differed from naïve at 1-wk IOP elevation, when it significantly increased for both nerve from KO-Ctrl and KO mice alike (Fig. 2 *C*, *Lower Right*). This is expected, since glycogen diminished significantly in both nerves for each strain compared to naïve at 1 wk (Fig. 2 *B*, *Right*). Importantly, for KO-ctrl nerves, changes in GPBB relative to naïve were opposite for IOP-stressed vs. contralateral: GPBB in IOP-stressed nerves diminished while increasing in the contralateral. This difference was significant at 4-d and 1-wk IOP elevation ($P \leq 0.04$). Cx43 KO reversed this trend significantly, so that GPBB in IOP-stressed nerves exceeded that of contralateral ($P \leq 0.04$), again consistent with less glycogen in stressed KO nerves (Fig. 2 *B*, *Right*). Thus, as with glycogen, astrocyte Cx43 contributes to the activation of metabolic pathways in both optic nerves following IOP elevation in one eye.

Not only does the presence of astrocyte Cx43 allow unilateral IOP elevation to activate AMPK across both visual streams, we also find it influences the distance Cx43-mediated astrocyte networks extend in both eyes. For this experiment, we utilized GFAP-GFP mice, with which we could distinguish astrocyte cell bodies in the retina among both their processes and Müller cell processes. We used these mice for patch-clamp recording and intracellular filling. Compared to naïve retina (Fig. 3*A*), the diffusion of gap junction-permeable dye (neurobiotin-350) injected into an astrocyte following 1 wk of unilateral elevation increased in the contralateral retina as it did in the IOP-stressed retina (Fig. 3 *B* and *C*). Diffusion within the retina was abolished by the gap junction blocker carbenoxolone (Fig. 3*D*). We confirmed the identity of single astrocytes marked for neurobiotin injection by their lack of action potentials in response to depolarizing voltage steps (Fig. 3*E*). Following injection, the most distant biotin-marked astrocyte (defined by a streptavidin signal greater than 20% above background that colocalized with GFAP in a soma) was significantly farther compared to naïve, not only for retina with IOP elevation, but also for the contralateral retina (Fig. 3*F*) ($^*P < 0.001$). Thus, unilateral IOP stress expands the astrocyte-coupled network in both retinas, allowing astrocytes to communicate quickly over greater distances.

To directly track the movement of glucose and its metabolites through the astrocyte network between the two eyes after unilateral injury, we elevated IOP in one eye and injected the radioactive glucose analog ^{18}F-FDG (fluorodeoxyglucose) intravitreally into the contralateral eye 1 wk later (Fig. 4*A*; IOP in *SI Appendix*, Fig. S1). Mice without microbead elevation served as control. One hour following ^{18}F-FDG injection, PET and CT scans showed how metabolites originating in the unstressed projection redistributed. In naïve WT mice without IOP elevation (Fig. 4*B*), transfer to the contralateral eye and nerve was minimal, only 1.24 ± 0.11% of the injected dose, typical of dissemination in neuronal tissues (42). Remarkably, a 1-wk IOP elevation in WT mice (Fig. 4*C*) increased contralateral transfer from the unstressed eye by 324%: 5.26 ± 1.06% of the injected dose ($P = 0.001$). Thus, IOP elevation has an extensive impact on metabolic state well beyond the directly stressed tissue, causing contralateral tissues to donate bioenergetic resources.

In KO-Ctrl mice, the transfer of ^{18}F-FDG to the IOP-stressed eye and nerve was not significantly different from WT (4.93 ± 1.01%; $P = 0.42$) (Fig. 4*D*). In KO mice, however, transfer of ^{18}F-FDG from the unstressed eye to the IOP-stressed eye and nerve was reduced such that KO-Ctrl transferred 272% more glucose than KO ($P < 0.001$) and did not differ from transfer in naïve KO mice without IOP elevation (1.33 ± 0.17 vs. 1.56 ± 0.13%; $P = 0.16$) (Fig. 4 *E* and *F*). Levels of ^{18}F-FDG contained in the bladder did not differ between any of the groups, indicating that in each a similar amount of metabolite reached the circulatory system ($P \geq 0.18$) (Fig. 4*H*). Additionally, transection of optic nerve that maintained they eye's vascular input prevented transfer of metabolites to the IOP-stressed contralateral projection (Fig. 4*I*). Metabolite transfer for WT sham was significantly elevated above transection (4.89 ± 1.46 vs. 0.78 ± 0.25; $P = 0.025$), resulting in contralateral ^{18}F-FDG values similar to that of WT microbead alone (Fig. 4 *J* and *K*). Both transection and sham conditions resulted in similar bladder ^{18}F-FDG content ($P = 0.48$) (Fig. 4*L*). Together, these results demonstrate that ^{18}F-FDG is redistributed from healthy to stressed tissue through an astrocyte Cx43-mediated network within the optic projection itself.

Optic Nerve Contralateral to Elevated IOP Exhibits Functional Deficits following Metabolic Challenge. Next, we investigated how metabolite transfer between optic projections influences physiological response to induced stress by recording the compound action potential (CAP) from WT and KO optic nerves ex vivo during glucose deprivation and recovery (Fig. 5). We measured the positive voltage response following brief depolarizing voltage pulses, typically in the first 40 to 80 ms following the pulse (Fig. 5*A*); the CAP itself was calculated as its integral (4, 8, 37, 43). After an initial period (15 min) of recording baseline CAP to determine each nerve's maximum, we depleted glucose via substitution with L-glucose, an enantiomer of glucose that is not metabolically utilized by living organisms because it cannot be phosphorylated by hexokinase, the first enzyme in the glycolysis pathway (44). Following glucose depletion for 1 h, we then measured the recovery in D-glucose for the following 30 min (Fig. 5 *A*, *Inset*).

The CAP for naïve KO optic nerve did not differ from that of naïve WT at any point, including an initial increase upon L-glucose substitution we attribute to glycogen mobilization ($P \geq 0.09$) (Fig. 5*B*). Following 1 wk of unilaterally elevated IOP (*SI Appendix*, Fig. S1), the WT CAP did not change compared to naïve ($P \geq 0.10$) (Fig. 5 *C* vs. *B*). However, the CAP for the unstressed contralateral nerve significantly diminished at 9 of 12 sampled times during glucose depletion ($P \leq 0.04$), including suppression of the initial rise in response, and recovered only to 45% of

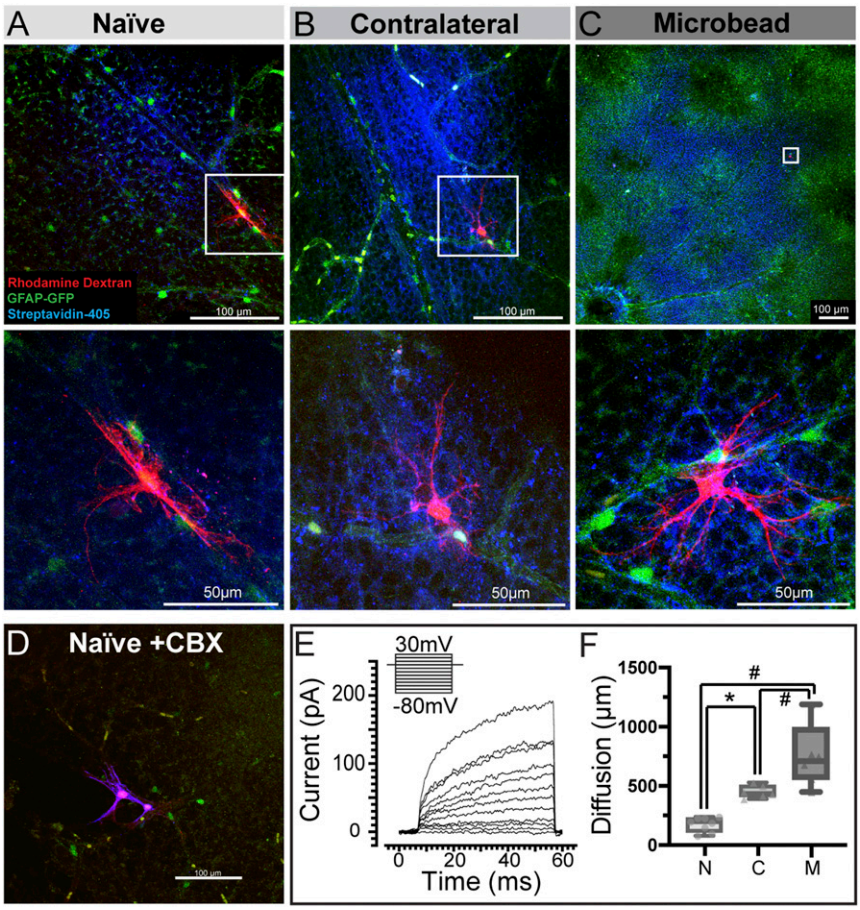

Fig. 3. Astrocyte coupling increases bilaterally after unilateral stress. Gap junction coupling of astrocytes in naïve (*A*), contralateral (*B*), and microbead (*C*) retinas following 1 wk of unilateral IOP elevation in GFAP-eGFP (green) mice. Coupling visualized by diffusion of neurobiotin (postlabeled with streptavidin-405, blue) dialyzed during patch-clamp physiological recording from astrocytes filled by injection of rhodamine dextran (red), which is too large to permeate gap junctions (67). *Lower* row shows higher magnification of boxed area. (*D*) When gap junctions were blocked with carbenoxolone (CBX), neurobiotin no longer transferred between astrocytes. (*E*) Current responses to voltage-steps (*Inset*) confirm astrocytes did not produce action potentials. (*F*) Distance to furthest neurobiotin-labeled astrocyte (biotin signal <20% above background and colocalized with GFAP-bearing cell body) from injected cell (identified with rhodamine dextran) significantly increased in contralateral and microbead retinas compared to naïve ($^{\#}P < 0.001$); coupling in microbead significantly greater than contralateral ($^{*}P = 0.007$).

baseline compared to 65% for the IOP-stressed nerve ($P \leq 0.04$) (Fig. 5*C*). Thus, the contralateral, putatively unstressed nerve exhibits a greater deficit in its physiological response to subsequent metabolic depletion than tissue directly stressed by IOP.

This pattern reversed in KO nerves (Fig. 5*D*). Elevated IOP eradicated the initial rise upon glucose depletion compared to naïve KO ($P \leq 0.04$) and IOP-stressed WT nerves ($P \leq 0.05$), as in the unstressed contralateral nerve in WT mice. With return to D-glucose, recovery of the CAP for IOP-stressed KO nerves did not differ from either naïve KO or IOP-stressed WT ($P \geq 0.220$, $P \geq 0.103$, respectively). In contrast to WT, the CAP from the unstressed contralateral nerve in KO mice exceeded that of the IOP-stressed nerve in the initial response to glucose depletion and in the final recovery (both $P \leq 0.04$). Remarkably, in KO mice the CAP for the unstressed contralateral nerve did not differ at any time from the naïve response ($P \geq 0.12$). As well, the CAP from the unstressed contralateral KO nerve exceeded that of the corresponding WT nerve at each point following glucose depletion ($P \leq 0.03$). Thus, metabolic redistribution through astrocyte Cx43 renders the donating tissue more susceptible to subsequent metabolic depletion but preserves physiological responses in the IOP-stressed tissue.

Conditional KO of Astrocyte Cx43 Accelerates Axonopathy and Functional Loss. Similar to other neurodegenerative diseases (45, 46), glaucoma involves deficits in axonal anterograde transport to central brain targets. This represents an early and sensitive degenerative outcome associated with elevated IOP (16). The ratio of hyperphosphorylated vs. phosphorylated intermediate filaments impedes active transport and is another early indicator of axonal pathology in human neurodegeneration (47). For KO-Ctrl mice, Western blots using antibodies against each epitope of intermediate filament (SMI34 and -31, respectively) demonstrate that this ratio increased after 4 d and 1 wk of elevation in the IOP-stressed nerve compared to naïve nerve, but did not differ from the unstressed contralateral nerve (Fig. 6*A*). In contrast, for KO mice at 1 wk the ratio of hyper- to phosphorylated neurofilaments was significantly greater in the microbead nerve compared to the unstressed contralateral nerve ($P = 0.003$). After 2 wk of unilateral IOP elevation, for KO-Ctrl mice the ratio in the unstressed contralateral nerve exceeded not only naïve, but also the microbead nerve. In contrast, the ratio in the unstressed KO nerve was significantly less than naïve and the IOP-stressed nerve. Therefore, astrocyte Cx43 contributes to bilateral transfer of IOP-related stress even at the level of neurofilament modifications in neuronal axons comprising the optic nerve.

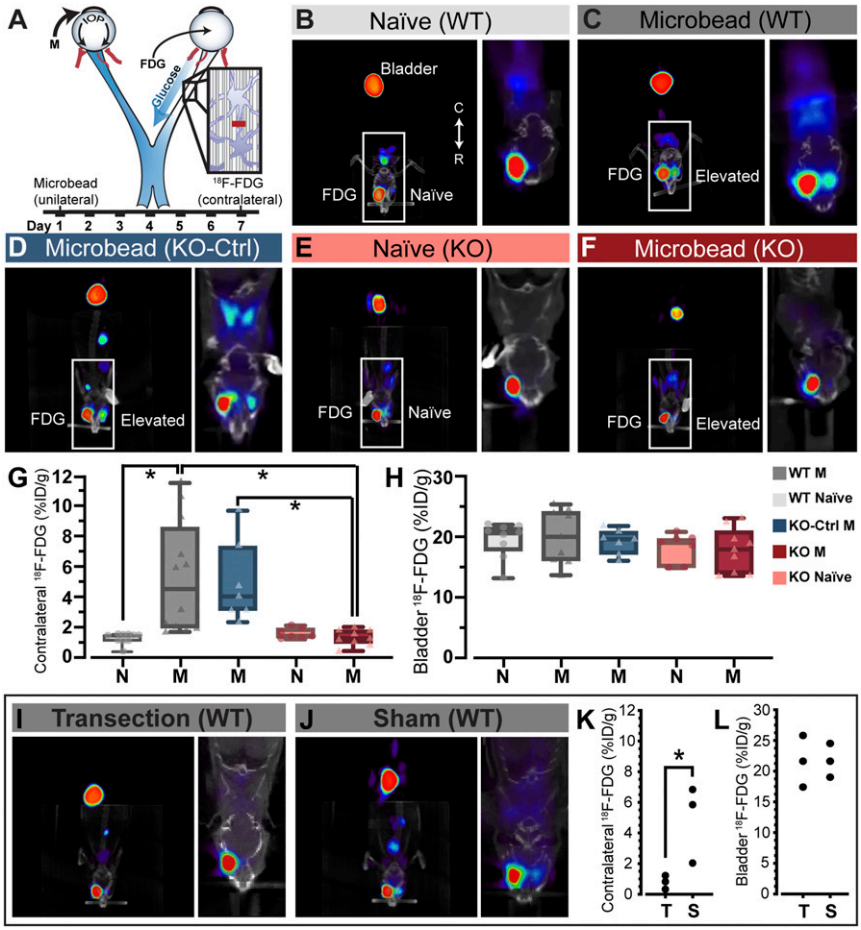

Fig. 4. IOP elevation causes metabolite transfer from unstressed tissue through astrocyte gap junctions. (*A*) One week of unilateral microbead-induced (M) IOP elevation in experimental (vs. naïve) mice followed by contralateral injection of ^{18}F-FDG, a radioactive glucose analog, to determine metabolite transfer between optic projections. (*B–F*) Representative PET (color) and CT (greyscale) images in naïve (*B*, $n = 10$) and microbead-elevated (*C*, $n = 12$) WT cohorts, microbead-elevated KO-Ctrl (*D*, $n = 7$), and naïve (*E*, $n = 11$) and microbead-elevated (*F*, $n = 7$) KO mice. (*G*) Unilateral IOP elevation in WT mice increased contralateral transfer from the unstressed eye by 324% (*$P < 0.001$). KO produced a 272% reduction in transferred ^{18}F-FDG compared to KO-Ctrl and WT (*$P < 0.001$). (*H*) Bladder radioactivity did not differ among groups. (*I*) When the donating nerve is transected in microbead-elevated mice prior to PET, metabolite transfer no longer occurs; sham surgery (*J*) does not impact metabolite transfer. (*K*) Metabolite transfer in the sham (S) condition was significantly elevated above transection (T; *$P = 0.025$). (*L*). Both transection and sham resulted in similar bladder ^{18}F-FDG content ($P = 0.48$).

From the preceding data, the contralateral optic nerve appears vulnerable to neurodegenerative stress after donating its energetic reserves. To test directly whether the contralateral nerve would progress through neurodegeneration more quickly if its fellow eye had already experienced a stressor, we tested axonal transport in vivo using three IOP-stressed cohorts of KO and KO-Ctrl mice (Fig. 6 *B*, *Top*, and *SI Appendix*, Fig. S2). A cohort with unilateral elevation was killed after 1 wk, while a second cohort was killed following 2 wk. In a third, staggered cohort, following 1 wk of IOP elevation in one eye, we elevated IOP in the contralateral eye and then killed after a further week. We then compared tissues that had experienced either 1 or 2 wk of elevation in this staggered, bilaterally stressed cohort to their corresponding unilateral controls. Both 1- and 2-wk elevations were significant compared to preexperiment IOP and to IOP in naïve eyes ($P < 0.001$), but did not differ in magnitude from one another ($P \geq 0.24$). Forty-eight hours prior to killing, all eyes received an injection of cholera toxin B (CTB) to assess the retinotopic representation of active axonal anterograde transport to the SC, the primary ganglion cell neuron target in rodents (32, 33).

The unilaterally stressed groups revealed intriguing differences in neuronal degeneration in the presence and absence of astrocyte Cx43. One-week unilateral IOP elevation did not affect the level of active transport compared to the unstressed contralateral SC in KO-Ctrl mice ($P = 0.35$) (Fig. 6 *B* and *C*, *Left*). In contrast, the same 1-wk elevation in KO mice reduced transport by 40% (59.6 ± 6.2%), significantly less than active transport both in the contralateral unstressed SC (91.6 ± 3.2% intact; $P = 0.002$) and in the corresponding KO-Ctrl SC ($P = 0.03$). For the 2-wk unilateral cohort (Fig. 6 *B* and *C*, *Center*), elevated IOP significantly reduced active transport in KO-Ctrl mice compared to the unstressed contralateral SC (68.8 ± 4.4% vs. 92.8 ± 2.1%; $P = 0.02$). Even so, transport degraded more dramatically in KO SC compared to its contralateral unstressed SC (48.2 ± 4.9% vs. 92.8 ± 1.9%; $P < 0.001$) and compared to the IOP-stressed SC in KO-Ctrl ($P = 0.01$). These differences in transport following unilateral IOP track well with changes in SMI34/31 ratio in the corresponding optic nerves (Fig. 6*A*) and demonstrate the impact of astrocyte networks on maintaining axonal function through neurodegenerative stress.

Astrocyte Cx43-mediated gap junctions proved even more important in our staggered, bilaterally stressed cohort. In the

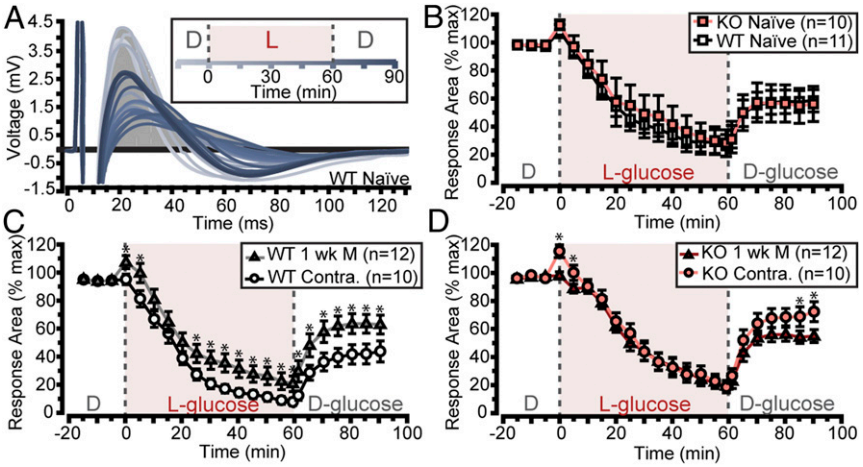

Fig. 5. Cx43 KO rescues contralateral CAP during glucose depletion. (*A*) CAP recorded at 5-min intervals as integral of positive voltage response (gray area) to depolarizing pulse. Measurements over 90 min (*Inset*) from baseline recordings (light blue) in D-glucose (*Inset*, D), glucose depletion with L-glucose (*Inset*, L, medium blue), and recovery in D-glucose (dark blue). (*B*) CAP for naïve WT and KO nerves did not differ ($P \geq 0.09$). (*C*) CAP for WT contralateral diminished compared to IOP-stressed nerve (*$P \leq 0.04$); KO rescues contralateral response compared to IOP-stressed nerve (*D*; *$P \leq 0.04$).

staggered cohort of animals that experienced a second IOP elevation affecting the contralateral, donating tissue, we found that astrocyte Cx43 allows the nervous system to distribute and equalize neurodegenerative outcomes between otherwise disparate regions. For this staggered KO-Ctrl cohort (Fig. 6 *B* and *C*, *Right*), degradation of transport to the SC subjected to 2-wk IOP elevation (M in Fig. 6 *B*, *Top*) did not differ significantly from the contralateral SC subjected to microbead elevation 1 wk later (MC in Fig. 6 *B*, *Top*) ($P = 0.41$), despite that eye experiencing only half the IOP elevation. However, the level of intact transport in both SCs significantly diminished compared to their unilateral counterparts, despite similar elevations in IOP (57.5 ± 2.9 and 51.4 ± 2.1, respectively; $P \leq 0.008$). Stressing both eyes caused each to be at a significant disadvantage when combating this neurodegenerative stressor, and particularly affected the tissue that had already donated resources to the originally stressed region.

This effect was absent for KO mice in the staggered cohort, where transport degradation in SC from neither the initial 2-wk elevation (M) nor the staggered contralateral 1 wk (MC) differed from deficits in the corresponding unilateral IOP elevation SC ($P \geq 0.11$). In addition, unlike KO-Ctrl SC, transport deficits for 2-wk elevation were significantly worse than the contralateral 1 wk (43.7 ± 5.2% vs. 61.3 ± 3.5% intact; $P = 0.04$). These findings suggest that resource redistribution through astrocyte Cx43 renders neurons within the donating tissue more susceptible to neurodegenerative damage during subsequent stressors. Additionally, by eliminating astrocyte Cx43, functional outcomes between the two projections were no longer equilibrated.

Finally, to determine whether Cx43 KO influences visual function after IOP elevation, we examined contrast spatial acuity via optomotor response (OMR) (Fig. 7). Acuity in KO-Ctrl eyes that received the initial microbead-induced IOP elevation (M) diminished 10% by day 6 compared to baseline (0.45 ± 0.01 vs. 0.51 ± 0.01 cycles/degree; $P < 0.001$), with a total decline of 20% by 2 wk (0.41 ± 0.01 cycles/degree, $P < 0.001$). Importantly, acuity in the KO-Ctrl contralateral eye that received subsequent IOP elevation for 1 wk (MC) declined by a similar amount from its baseline, but in half the time (0.40 ± 0.01 vs. 0.51 ± 0.01 cycles/degree; $P < 0.001$). Final acuity in the two KO-Ctrl eyes did not differ ($P = 0.33$) despite differences in the duration of IOP elevation, as with axon transport (Fig. 6).

For KO eyes receiving the initial IOP elevation (M), the initial decrease in spatial acuity by day 6 was twofold worse than KO-Ctrl (0.39 ± 0.10 vs. baseline 0.50 ± 0.01 cycles/degree; $P < 0.001$), reaching a total decline in acuity of 39% over the 2-wk period (0.31 ± 0.02 cycles/degree; $P < 0.001$). Acuity in the contralateral KO eye receiving IOP elevation a week later (MC) remained at baseline levels 2 d following elevation (0.50 ± 0.02 cycles/degree, $P = 0.41$), even though by this time the same eye in the KO-Ctrl cohort diminished compared to its baseline (0.46 ± 0.01 cycles/degree; $P < 0.001$). While the difference in acuity between the KO and KO-Ctrl contralateral eyes at day 9 was significant ($P = 0.009$), by day 14, acuity for these eyes no longer differed ($P = 0.15$), due to a 25% decrease for the KO eye ($P < 0.001$). In fact, this decrease—1 wk following its elevation—brought acuity for the KO contralateral eye to a level not significantly different from the KO fellow eye at its 1-wk elevation point ($P = 0.31$). Thus, although isolating each visual stream from the broader astrocyte network transiently protected the contralateral nerve from subsequent damage, both the initially stressed and contralateral KO visual streams eventually demonstrated visual acuity either equivalent to or even worse than both control conditions.

Discussion

Astrocytes are the most numerous cell type in the central nervous system, forming interconnected networks mediated by gap junctions primarily composed of Cx43. Astrocyte gap junctions have been implicated in a variety of neurodegenerative conditions (28, 30), but the beneficial aspects of gap junction alterations through disease progression are less well understood. As neurons signal and utilize their metabolites under healthy conditions, local astrocyte gap junctions allow mobilization of stored energetic reserves (31, 48). To determine the mechanism by which these energetic reserves are mobilized during disease, we utilized conditional mutagenesis of floxed *Cx43* with the tamoxifen-inducible *Cre-ER^{T2}* under a GFAP promoter (*GFAP-Cre-ER^{T2}* × *Cx43$^{flox/flox}$*). We found astrocyte gap junction-mediated networks influence metabolite distribution more globally, between distant regions of the optic projection during stress induced by elevated IOP.

Sensitivity to IOP is a defining feature of axonal degeneration in the optic nerve during glaucoma (17), which also involves enhanced neuronal excitation early in progression (49). Our fundamental finding is that in response to IOP elevation in one eye, astrocyte gap junctions redistribute metabolic resources from the other optic projection, across the large distance separating the two eyes (Fig. 4). While beneficial to the stressed optic projection, redistribution renders contralateral donating tissue

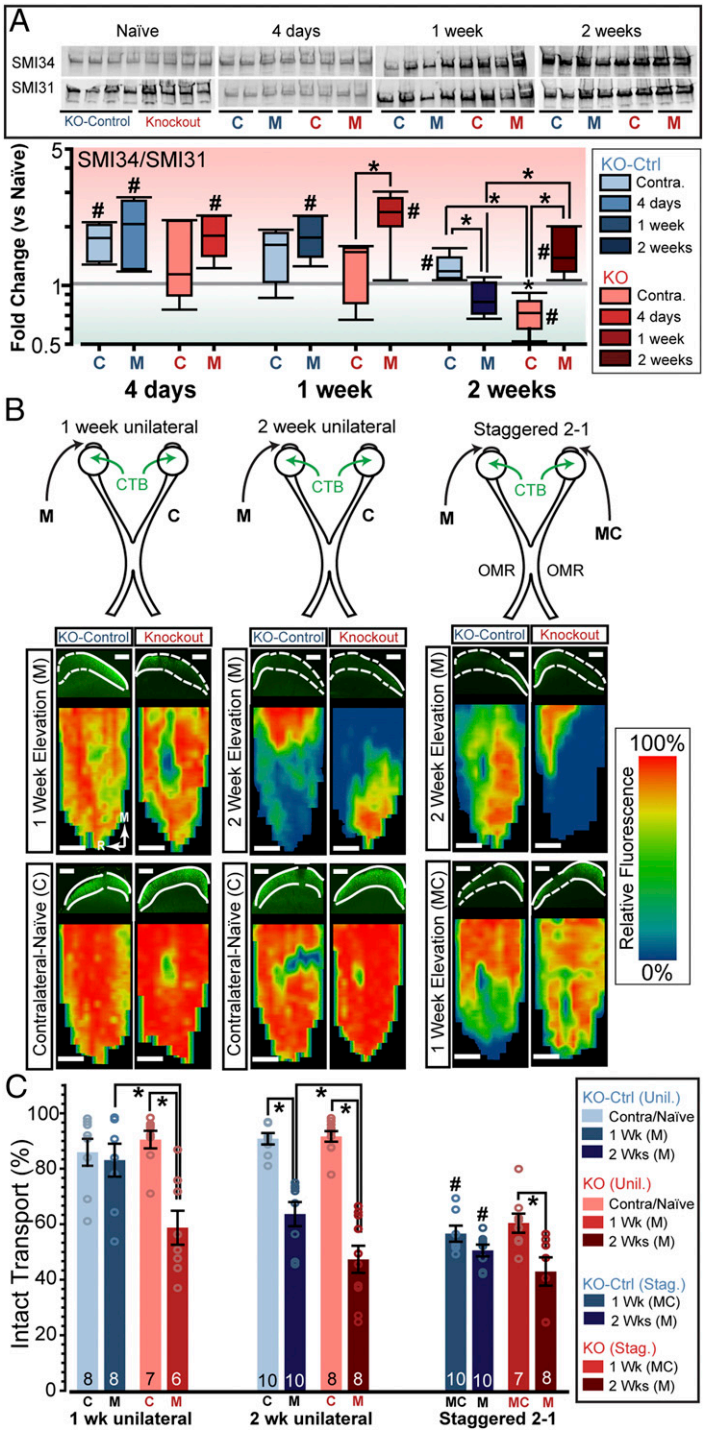

Fig. 6. Cx43 KO accelerates axonopathy in the optic projection. (*A*, *Upper*) Western blots probing hyperphosphorylated (SMI34) and phosphorylated (SMI31) intermediate filaments in KO and KO-Ctrl optic nerves following unilateral IOP elevation. (*Lower*) For KO-Ctrl, the ratio of SMI34/31 increased significantly over genotype naïve (#; Ctrl SEM $\pm$ 0.09, KO SEM $\pm$ 0.22) in both microbead and contralateral nerves after 4 d of unilateral elevation ($n = 5$), in microbead at 1 wk ($n = 6$), and in the contralateral nerve at 2 wk ($n = 5$). At 2 wk, KO-Ctrl microbead was less than its contralateral and the KO microbead (*). For KO microbead, SMI34/31 exceeded its genotype naïve at 4 d ($n = 5$), 1 and 2 wk ($n = 8, 5$). In contrast to KO-Ctrl, at 2 wk KO microbead exceeded naïve while contralateral was less (#). $^{\#}P \leq 0.02$; $^{*}P \leq 0.006$. (*B*, *Top*) Contralateral (C) eye is naïve for unilateral 1- and 2-wk IOP elevations via microbead (M) injection, in staggered cohort (*Right*), contralateral received microbead injection (MC) 1 wk later. Both eyes underwent OMR assessment. All eyes received CTB prior to killing. IOPs in *SI Appendix*, Fig. S2. (*Bottom*) Coronal section (*Middle*) through SC demonstrating intact (solid white line) vs. degraded (dashed) anterograde transport. Reconstructed SC retinotopic maps range from 100% (red) to 0% (blue) transport. M: medial; R: rostral. (Scale bars, 500 μm.) (*C*) Intact transport (percent map with ≥70% CTB) for KO-Ctrl vs. KO in 1-wk (*Left*), 2-wk (*Center*), and staggered (*Right*) cohorts. One-week elevation in KO mice reduced transport vs. the contralateral SC ($^{*}P = 0.002$) and vs. the corresponding KO-Ctrl SC ($^{*}P = 0.03$). Two weeks reduced transport in KO-Ctrl ($^{*}P = 0.020$) and KO ($^{*}P < 0.001$) vs. unstressed contralateral, while KO deficits exceeded KO-Ctrl ($^{*}P = 0.01$). In the staggered cohort, transport reduced after 1-wk (MC) and 2-wk (M) elevations in KO-Ctrl vs. unilateral 1- and 2-wk ($^{\#}P \leq 0.008$) and in 2- (M) vs. 1-wk (MC) KO SC ($^{*}P = 0.04$).

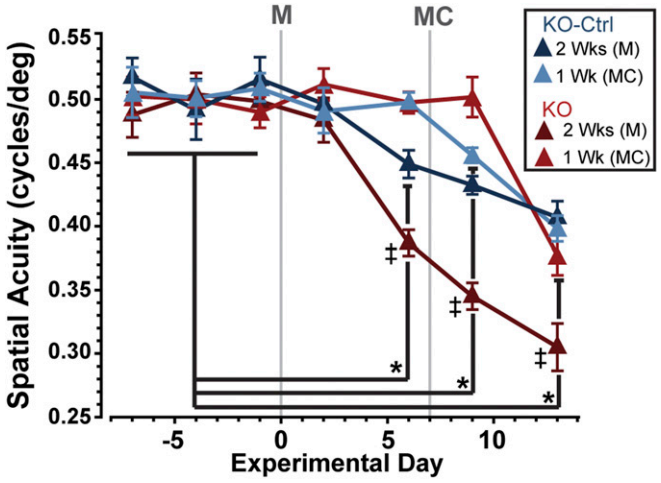

Fig. 7. Cx43 KO causes rapid deterioration of visual function. Spatial acuity (cycles/degree) determined from OMR for KO-Ctrl (n = 9) and KO (n = 10) mice in staggered cohort following initial microbead injection (M, arrow) and subsequent injection in contralateral eye (MC, arrow); IOP in *SI Appendix*, Fig. S2. Acuity did not differ for the first four measurements in any group ($P \geq 0.11$). Acuity in eye with first elevation (M) for KO-Ctrl and KO diminished below baseline by day 6 (*$P < 0.001$); decline in KO acuity was worse than KO-Ctrl ($^{‡}P < 0.001$). For KO-Ctrl, acuity in the contralateral eye (MC) diminished below baseline by day 9 and continued to decline until the final measurement (*$P < 0.001$), where it reached acuity in the M eye (P = 0.33). For MC KO eyes, acuity remained above M eye throughout ($P < 0.001$) and did not decline from baseline until the final measurement (*$P < 0.001$).

more susceptible to further stressors (Figs. 3, 6, and 7). Bilateral glial activation after unilateral optic nerve stress has been observed previously (50), in microglia (51) as well as astrocytes (52). One study (50) confirmed bilateral axonal loss after unilateral optic nerve crush, finding similarities in the contralateral nerve to an incomplete crush and postulating an adaptive function wherein the SC equilibrated inputs from both eyes. We too found evidence that when the donating tissue is exposed to elevated IOP after it has donated its energetic reserves, functional outcomes are equilibrated between the two optic projections. Equilibration no longer occurred following astrocyte Cx43 KO, implying that astrocyte connectivity is necessary for this process. There is evidence in human glaucoma progression as well for extensive cross-talk between the two optic projections that produces a complete bilateral visual field by fusing the fragmented, yet complementary representations from the two eyes (53).

While Cx43 may be retained in vascular endothelial cells, in retinal Müller glia, or in astrocytes due to variability in Cre-ER^{T2} induction, our transgenic experiment yielded significant reduction of astrocyte Cx43 in the retina and optic projection (Fig. 1), which otherwise is elevated in glaucoma (30). Optic nerve stress from elevated IOP in glaucoma involves diminished ATP and other metabolic challenges that contribute to early axon dysfunction, including degradation of anterograde transport to the brain (15–18). We found IOP elevation for only 1 wk influences protein expression in the unstressed, contralateral optic nerve, increasing stress-response proteins, glycogen catabolism, and hyperphosphorylation of neurofilaments (Figs. 2 and 6). This induced contralateral response travels as far as the opposite eye, where the coupled retinal astrocyte network more than doubles in size compared to naïve (Fig. 3).

In WT and KO-Ctrl tissues, we see that glycogen stores in the contralateral optic nerve diminish more than their counterparts ipsilateral to IOP elevation. In GFAP-driven Cx43 KO mice, this pattern reverses; after 1 wk of elevation, glycogen in the ipsilateral nerve is significantly diminished compared to that in the contralateral nerve (Fig. 2*B*). This reversal was significant, but not complete; the contralateral tissue still showed a significant loss of glycogen when compared to naïve tissues. This may be from the nature of a tamoxifen-induced KO, which is unlikely to have induced excision in every GFAP-expressing astrocyte. Additionally, GFAP expression and transcription varies greatly across astrocytes (54), so by its nature our KO would not reach every astrocyte in the brain. Incomplete reversal may also be due to resource donation through other connexins astrocytes may express (29). Each of these factors could contribute to the amount of resource donation and glycogen loss we still detect in the contralateral tissue. That these findings were still of such magnitude speaks to the remarkable capacity of astrocyte Cx43-mediated networks.

Intriguingly, the pAMPK/AMPK ratio in our GFAP-driven Cx43 KO mice did not increase (Fig. 2*C*), even in the nerve corresponding to the stressed eye. This may be due in part to the composition of the optic nerve itself, which is mostly glia (41). Within retinal ganglion cells, pAMPK additionally appears to be localized somatically rather than within the axon in glaucoma models (55). Furthermore, in a chronic mouse model of glaucoma, AMPK within the optic nerve is primarily localized and phosphorylated within astrocytes rather than axons (18). Without the majority of their gap junctions, optic nerve astrocytes may be unable to detect IOP stress, reflecting greater isolation than anticipated.

Metabolite redistribution (as measured by ^{18}F-FDG PET imaging) from unstressed to stressed optic projections after elevated IOP requires Cx43-mediated astrocyte coupling, since conditional KO inhibits redistribution (Fig. 4*G*). This coupling likely allows transfer via the optic chiasm, where the predominantly contralateral projections from the two eyes cross (41). When the experiment is repeated but the contralateral optic nerve is transected, metabolites no longer transfer between the two projections, but still circulate through the bloodstream to the same extent as the sham condition (Fig. 4 *K* and *L*). Similar metabolic transfer occurs in corpus callosum, with astrocytes and oligodendrocytes coupling in response to glucose deprivation to maintain action potential generation (56, 57).

Both the speed at which metabolites migrate and the relative deficit in glycogen within the unstressed compared to stressed nerve imply an active process. A relative metabolic "sink" in the stressed tissue could explain the eventual equilibrium between the two nerves we see after 4 but not 1 or 2 wk of elevation. Perhaps through a heterotypic connexin configuration (28, 58) astrocytes can dynamically regulate the flow of ions and molecules through their network. Another possibility involves the charge of the metabolites specifically traced here, which all derive from glucose, the brain's main source of energy (3). Glucose and the metabolites derived from it are polar molecules (59), subject to interaction with other charged entities, such as calcium ions that could influence their flow.

Our results show that nerves contralateral to short-term (1 wk) unilateral IOP elevation exposed to a further metabolic stressor ex vivo exhibit much weaker compound action potential than their directly stressed counterparts (Fig. 5). In the KO this pattern reverses, with the directly stressed nerve demonstrating a weaker signal than its contralateral counterpart. This finding suggests that astrocyte-mediated transfer of metabolites between projections depletes the donor tissue and renders it susceptible to further metabolic stressors. Yet, astrocyte Cx43 KO reduced physiological measures of visual function in the directly stressed tissue extensively, including both active anterograde transport to the SC (Fig. 6) and visual acuity (Fig. 7), indicating the systemic importance of Cx43 gap junction-mediated mobilization of metabolic resources. Even the donating KO-Ctrl tissue, which indeed was more susceptible to neurodegenerative stress initially

following IOP elevation, still demonstrated more intact visual function than its KO counterpart after 6 d of elevation (Fig. 7). These results demonstrate that metabolic components of the Cx43 astrocyte network are critical for maintaining function bilaterally early in neurodegenerative disease (Fig. 8). By comparison, pharmacological blockade of neuronal gap junctions generally or genetic knockdown of connexin 36 (Cx36), which links retinal neurons of specific types to one another, significantly slowed retinal and nerve degeneration in the same model of glaucoma (60). Thus, retinal and nerve gap junctions serve multiple purposes, depending on whether coupling is glial (Cx43) or neuronal (Cx36).

Astrocyte Cx43 serves a number of important purposes in addition to metabolic redistribution worthy of consideration. Unpaired connexins have the capacity to act as hemichannels, opening to the extracellular space rather than to an individual cell (61). These hemichannels release gliotransmitters (such as glutamate) (62), facilitate purinergic signaling (63), and release molecules such as nicotinamide adenine dinucleotide and D-serine into the extracellular milieu (64). Paired gap junctions formed by Cx43 can transmit other molecules and ions as well, provided the molecules are generally below 1 to 1.2 kDa (28), including the well-documented example of calcium signaling (65). Each of these functions would also be disturbed in our KO and could have contributed to our results.

Evolving evidence suggests that astrocyte reactivity in response to disease-relevant stress, although most often considered pathogenic, also includes protective outcomes (66). Our results demonstrate that local neurodegenerative stress induces a much broader astrocyte response capable of mediating metabolic redistribution across bilateral regions of the central nervous system. That the donating, contralateral optic nerve itself becomes vulnerable to subsequent metabolic stress could help explain how neurodegeneration in other age-related neurodegenerative diseases spreads from affected to unaffected tissues over time.

Summary of Methods

For detailed methods, please reference *SI Appendix, SI Methods*.

Animals. Adult (2 mo) C57/BL6 (male; Charles River Laboratory) and *GFAP-Cre-ER^{T2}* x *Cx43$^{flox/flox}$* mice (counterbalanced male/female) were maintained in a 12-h light/dark cycle with standard rodent chow and water available ad libitum. Tails snips were genotyped via PCR for *GFAP-Cre-ER^{T2}* (for CRE: forward, 5′ GCCAGTCTAGCCCACTCCTT 3′; reverse, 5′ TCCCTGAAC ATGTCCATCAG 3′; for internal positive control: forward, 5′ CTAGGCCACAGA ATTGAAAGATCT 3′; reverse 5′ GTAGGTGGAAATTCTAGCATCATCC 3′) and *Cx43$^{flox/flox}$* (forward, 5′ CTTTGACTCTGATTACAGAGCTTAA 3′; reverse, 5′ GTCTCACTGTTACTTAACAGCTTGA 3′). Experimental mice received 3 d of oral gavage tamoxifen in corn oil at 20 mg/mL, 10 μL/g of mouse; control mice received corn oil. Conventional PCR verified KO in cerebellum and tissues of interest in every mouse (forward, GCTACTTCTTGCTTTGACTCTGAT TA; reverse, GCTCACTTGATAGTCCACTCTAAGC), with 70.7% of tamoxifen-gavaged mice exhibiting successful excision. Controls that exhibited *Cx43$^{flox/flox}$* excision were excluded, but only 2 of 145 exhibited such recombination.

Microbead occlusion (38) elevated IOP in all conditions was measured via rebound tonometry (Tono-Pen XL, Medtronic Solan) (38). A subset of animals was bilaterally injected intravitreally with 2 μL of 0.5 mg CTB conjugated to Alexa Fluor 488 (Invitrogen). Intact transport within serial coronal SC sections was quantified as described previously (16).

Immunohistochemistry. Perfused (4% PFA) whole-mount retinas as well as 10-μm cryosections of optic nerve and 50-μm cryosections of SC were immunolabeled against GFAP (goat 1:500; Abcam) and Cx43 (rabbit 1:500; Cell Signaling Technology). Confocal micrographs were obtained using an Olympus FV-1000 inverted microscope.

Glycogen Assay. Glycogen content was determined by modifying Abcam assay ab65620. Tissue processing is detailed in *SI Appendix, SI Methods*.

Western Blotting. Gels were loaded with 10 μg of protein per well from individual optic nerves. Blots were incubated against AMPK (Cell Signaling antibody #2603; 1:1,000), pAMPK (Cell Signaling antibody #2535; 1:1,000), GPBB (GeneTex Cat No. GTX104291; 1:2,000), SMI34 (Biolegend #835501; 1:2,000), and SMI31 (Biolegend #801601; 1:2,000).

Electrophysiology. Retinas were prepared as previously described (49) and detailed in *SI Appendix*. Following recording and injection with a solution containing 1 mM Neurobiotin 350 (Vector Biolabs) and 1 mM dextran tetramethylrhodamine 3000 MW (Invitrogen), retinas were postfixed overnight in 4% PFA, then incubated in a solution containing Streptavidin-405. Confocal micrographs were obtained using an Olympus FV-1000 inverted microscope.

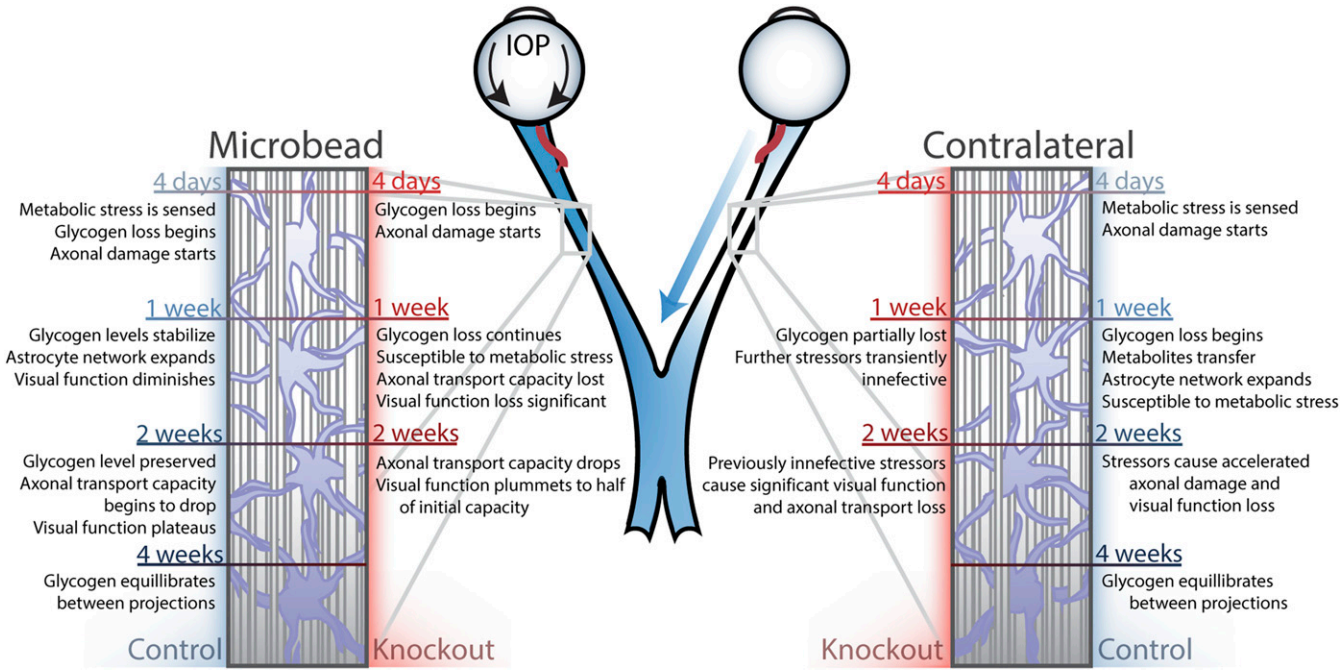

Fig. 8. Summary. KO and control experimental results summarized. For a full table of specific results, see *SI Appendix*, Table S1.

The distance between the patched cell (identified with rhodamine-dextran) and the most distant coupled astrocyte (identified as a cell body containing GFP and Streptavidin-405 20% above background) was measured.

Compound action potentials were initially evoked by voltage pulses every 30 s. Stimulus strength was adjusted to evoke the maximal-amplitude CAP, then increased 25% to ensure stimulus strength was supramaximal. All subsequent CAPs were evoked every 5 min over 1 h and 45 min, during which the bath solution was replaced with L-glucose artificial cerebrospinal fluid to determine the response to metabolic stress and again replaced with D-glucose artificial cerebrospinal fluid to determine recovery.

Positron Emission Tomography. We utilized a Siemens Inveon PET scanner (Siemens Preclinical), a NanoSPECT/CT (Bioscan), and the radioactive glucose analog ^{18}F-FDG. Mice were briefly anesthetized with 2.5% isoflurane and unilaterally intravitreally injected with 1.4 to 4.2 MBq/2 μL of ^{18}F-FDG. Animals were then returned to their cages and fed ad libitum for 60 min. Animals were again anesthetized with 2% isoflurane and imaged for 40 min in the Inveon microPET in static mode. PET and CT images were normalized to the injected radioactive dose of ^{18}F-FDG. Regions-of-interest (ROIs) were drawn as 7 × 14 × 7-mm cubes around the entire optic projection contralateral to ^{18}F-FDG injection, and mean radiotracer concentrations within the top 90% of voxels within ROIs were measured in units of percent injected dose per unit volume (%ID/g).

OMR Testing. Visual acuity was measured as described previously (49) (OptoMotry; CerebralMechanics Inc.).

Statistics. Data are presented as mean ± SEM for each treatment presented as bar or line graphs; box plots are presented with median, 10th, 25th, 75th, and 90th percentiles indicated. One-way ANOVAs or *t* tests were performed as appropriate as one-tailed tests (SigmaPlot 12.5; Systat Software). ANOVAs showing significance ($P < 0.05$) were followed by Tukey's (parametric) or Dunn's (nonparametric) post hoc comparisons. If data distributions violated two or more of the assumptions of ANOVA (normality of residuals, equal variances, and independent sampling), ANOVAs on ranked data were utilized. Before statistical analysis of dependent variables, data were assessed for outliers using Grubbs' test (GraphPad).

Data Reporting and Availability. All procedures were conducted in accordance with the animal care standards of the National Institute of Health and approved by the Vanderbilt University Medical Center Institutional Animal Care and Use Committee. All experiments were performed blindly with regard to mouse genotype. All data are included in the paper and *SI Appendix*. Reagents and other materials utilized herein, including transgenic mouse strains, are available from the corresponding author upon reasonable request.

ACKNOWLEDGMENTS. We thank Moses Chao for his thoughtful comments on the manuscript. Support for this study was provided by the Research to Prevent Blindness Stein Innovation Award; the Stanley Cohen Innovation Fund, and NIH RO1 Grants EY017427 and EY024997, T32 Grants EY021453 and EY007135, and P30 Grant EY008126 (Vanderbilt Vision Research Center). Imaging was supported through the Vanderbilt University Medical Center Cell Imaging Shared Resource core facility and NIH Grants CA68485, DK20593, DK58404, DK59637, and EY08126. The Inveon microPET scanner was funded through NIH OD01624 and the NanoSPECT/CT funded by RR023784-01.

1. J. M. Duarte, F. M. Girault, R. Gruetter, Brain energy metabolism measured by (13)C magnetic resonance spectroscopy in vivo upon infusion of [3-(13)C]lactate. *J. Neurosci. Res.* **93**, 1009–1018 (2015).
2. A. Falkowska *et al*., Energy metabolism of the brain, including the cooperation between astrocytes and neurons, especially in the context of glycogen metabolism. *Int. J. Mol. Sci.* **16**, 25959–25981 (2015).
3. P. Mergenthaler, U. Lindauer, G. A. Dienel, A. Meisel, Sugar for the brain: The role of glucose in physiological and pathological brain function. *Trends Neurosci.* **36**, 587–597 (2013).
4. A. M. Brown *et al*., Astrocyte glycogen metabolism is required for neural activity during aglycemia or intense stimulation in mouse white matter. *J. Neurosci. Res.* **79**, 74–80 (2005).
5. R. A. Swanson, M. M. Morton, S. M. Sagar, F. R. Sharp, Sensory stimulation induces local cerebral glycogenolysis: Demonstration by autoradiography. *Neuroscience* **51**, 451–461 (1992).
6. P. Hasel *et al*., Neurons and neuronal activity control gene expression in astrocytes to regulate their development and metabolism. *Nat. Commun.* **8**, 15132 (2017).
7. M. Bélanger, I. Allaman, P. J. Magistretti, Brain energy metabolism: Focus on astrocyte-neuron metabolic cooperation. *Cell Metab.* **14**, 724–738 (2011).
8. S. B. Tekkök, A. M. Brown, R. Westenbroek, L. Pellerin, B. R. Ransom, Transfer of glycogen-derived lactate from astrocytes to axons via specific monocarboxylate transporters supports mouse optic nerve activity. *J. Neurosci. Res.* **81**, 644–652 (2005).
9. A. Suzuki *et al*., Astrocyte-neuron lactate transport is required for long-term memory formation. *Cell* **144**, 810–823 (2011).
10. Y. Zhao *et al*., Decreased glycogen content might contribute to chronic stress-induced atrophy of hippocampal astrocyte volume and depression-like behavior in rats. *Sci. Rep.* **7**, 43192 (2017).
11. P. J. Magistretti, I. Allaman, Lactate in the brain: From metabolic end-product to signalling molecule. *Nat. Rev. Neurosci.* **19**, 235–249 (2018).
12. D. J. Rossi, J. D. Brady, C. Mohr, Astrocyte metabolism and signaling during brain ischemia. *Nat. Neurosci.* **10**, 1377–1386 (2007).
13. D. Vilchez *et al*., Mechanism suppressing glycogen synthesis in neurons and its demise in progressive myoclonus epilepsy. *Nat. Neurosci.* **10**, 1407–1413 (2007).
14. L. Mosconi, A. Pupi, M. J. De Leon, Brain glucose hypometabolism and oxidative stress in preclinical Alzheimer's disease. *Ann. N. Y. Acad. Sci.* **1147**, 180–195 (2008).
15. L. Coughlin, R. S. Morrison, P. J. Horner, D. M. Inman, Mitochondrial morphology differences and mitophagy deficit in murine glaucomatous optic nerve. *Invest. Ophthalmol. Vis. Sci.* **56**, 1437–1446 (2015).
16. S. D. Crish, R. M. Sappington, D. M. Inman, P. J. Horner, D. J. Calkins, Distal axonopathy with structural persistence in glaucomatous neurodegeneration. *Proc. Natl. Acad. Sci. U.S.A.* **107**, 5196–5201 (2010).
17. D. J. Calkins, Critical pathogenic events underlying progression of neurodegeneration in glaucoma. *Prog. Retin. Eye Res.* **31**, 702–719 (2012).
18. D. M. Inman, M. Harun-Or-Rashid, Metabolic vulnerability in the neurodegenerative disease glaucoma. *Front. Neurosci.* **11**, 146 (2017).
19. C. F. Burgoyne, A biomechanical paradigm for axonal insult within the optic nerve head in aging and glaucoma. *Exp. Eye Res.* **93**, 120–132 (2011).
20. C. Dai *et al*., Structural basis of glaucoma: The fortified astrocytes of the optic nerve head are the target of raised intraocular pressure. *Glia* **60**, 13–28 (2012).
21. M. Pazos *et al*., Expansions of the neurovascular scleral canal and contained optic nerve occur early in the hypertonic saline rat experimental glaucoma model. *Exp. Eye Res.* **145**, 173–186 (2016).
22. H. A. Quigley, A. T. Broman, The number of people with glaucoma worldwide in 2010 and 2020. *Br. J. Ophthalmol.* **90**, 262–267 (2006).
23. M. L. Cooper, S. D. Crish, D. M. Inman, P. J. Horner, D. J. Calkins, Early astrocyte redistribution in the optic nerve precedes axonopathy in the DBA/2J mouse model of glaucoma. *Exp. Eye Res.* **150**, 22–33 (2016).
24. M. L. Cooper, J. W. Collyer, D. J. Calkins, Astrocyte remodeling without gliosis precedes optic nerve axonopathy. *Acta Neuropathol. Commun.* **6**, 38 (2018).
25. M. A. Fazio *et al*., Regional variations in mechanical strain in the posterior human sclera. *Invest. Ophthalmol. Vis. Sci.* **53**, 5326–5333 (2012).
26. R. Grytz, I. A. Sigal, J. W. Ruberti, G. Meschke, J. C. Downs, Lamina cribrosa thickening in early glaucoma predicted by a microstructure motivated growth and remodeling approach. *Mech. Mater.* **44**, 99–109 (2012).
27. I. A. Sigal *et al*., IOP-induced lamina cribrosa deformation and scleral canal expansion: Independent or related? *Invest. Ophthalmol. Vis. Sci.* **52**, 9023–9032 (2011).
28. C. Giaume, C. C. Naus, Connexins, gap junctions, and glia. *Wiley Interdiscip. Rev. Membr. Transp. Signal.* **2**, 133–142 (2013).
29. R. Dermietzel *et al*., Connexin43 null mice reveal that astrocytes express multiple connexins. *Brain Res. Brain Res. Rev.* **32**, 45–56 (2000).
30. N. M. Kerr, C. S. Johnson, C. R. Green, H. V. Danesh-Meyer, Gap junction protein connexin43 (GJA1) in the human glaucomatous optic nerve head and retina. *J. Clin. Neurosci.* **18**, 102–108 (2011).
31. N. Rouach, A. Koulakoff, V. Abudara, K. Willecke, C. Giaume, Astroglial metabolic networks sustain hippocampal synaptic transmission. *Science* **322**, 1551–1555 (2008).
32. B. Dreher, A. J. Sefton, S. Y. Ni, G. Nisbett, The morphology, number, distribution and central projections of class I retinal ganglion cells in albino and hooded rats. *Brain Behav. Evol.* **26**, 10–48 (1985).
33. E. M. Ellis, G. Gauvain, B. Sivyer, G. J. Murphy, Shared and distinct retinal input to the mouse superior colliculus and dorsal lateral geniculate nucleus. *J. Neurophysiol.* **116**, 602–610 (2016).
34. C. M. Alberini, E. Cruz, G. Descalzi, B. Bessières, V. Gao, Astrocyte glycogen and lactate: New insights into learning and memory mechanisms. *Glia* **66**, 1244–1262 (2018).
35. A. M. Brown, B. R. Ransom, Astrocyte glycogen and brain energy metabolism. *Glia* **55**, 1263–1271 (2007).
36. I. Allaman *et al*., Amyloid-beta aggregates cause alterations of astrocytic metabolic phenotype: Impact on neuronal viability. *J. Neurosci.* **30**, 3326–3338 (2010).
37. R. Wender *et al*., Astrocytic glycogen influences axon function and survival during glucose deprivation in central white matter. *J. Neurosci.* **20**, 6804–6810 (2000).
38. R. M. Sappington, B. J. Carlson, S. D. Crish, D. J. Calkins, The microbead occlusion model: A paradigm for induced ocular hypertension in rats and mice. *Invest. Ophthalmol. Vis. Sci.* **51**, 207–216 (2010).
39. A. Heijl *et al*.; Early Manifest Glaucoma Trial Group, Reduction of intraocular pressure and glaucoma progression: Results from the early manifest glaucoma trial. *Arch. Ophthalmol.* **120**, 1268–1279 (2002).
40. C. Cantó *et al*., AMPK regulates energy expenditure by modulating NAD+ metabolism and SIRT1 activity. *Nature* **458**, 1056–1060 (2009).
41. J. A. Perge, K. Koch, R. Miller, P. Sterling, V. Balasubramanian, How the optic nerve allocates space, energy capacity, and information. *J. Neurosci.* **29**, 7917–7928 (2009).

42. V. Berti, L. Mosconi, A. Pupi, Brain: Normal variations and benign findings in fluorodeoxyglucose-PET/computed tomography imaging. *PET Clin.* **9**, 129–140 (2014).
43. N. Meyer *et al*., Oligodendrocytes in the mouse corpus callosum maintain axonal function by delivery of glucose. *Cell Rep.* **22**, 2383–2394 (2018).
44. A. Tabernero, C. Giaume, J. M. Medina, Endothelin-1 regulates glucose utilization in cultured astrocytes by controlling intercellular communication through gap junctions. *Glia* **16**, 187–195 (1996).
45. G. B. Stokin *et al*., Axonopathy and transport deficits early in the pathogenesis of Alzheimer's disease. *Science* **307**, 1282–1288 (2005).
46. S. Millecamps, J. P. Julien, Axonal transport deficits and neurodegenerative diseases. *Nat. Rev. Neurosci.* **14**, 161–176 (2013).
47. A. Petzold *et al*., Phosphorylation and compactness of neurofilaments in multiple sclerosis: Indicators of axonal pathology. *Exp. Neurol.* **213**, 326–335 (2008).
48. N. Rouach, J. Glowinski, C. Giaume, Activity-dependent neuronal control of gap-junctional communication in astrocytes. *J. Cell Biol.* **149**, 1513–1526 (2000).
49. M. L. Risner, S. Pasini, M. L. Cooper, W. S. Lambert, D. J. Calkins, Axogenic mechanism enhances retinal ganglion cell excitability during early progression in glaucoma. *Proc. Natl. Acad. Sci. U.S.A.* **115**, E2393–E2402 (2018).
50. T. Macharadze *et al*., Interretinal transduction of injury signals after unilateral optic nerve crush. *Neuroreport* **20**, 301–305 (2009).
51. L. P. Cen *et al*., Bilateral retinal microglial response to unilateral optic nerve transection in rats. *Neuroscience* **311**, 56–66 (2015).
52. N. Bodeutsch, H. Siebert, C. Dermon, S. Thanos, Unilateral injury to the adult rat optic nerve causes multiple cellular responses in the contralateral site. *J. Neurobiol.* **38**, 116–128 (1999).
53. W. E. Sponsel, S. L. Groth, N. Satsangi, T. Maddess, M. A. Reilly, Refined data analysis provides clinical evidence for central nervous system control of chronic glaucomatous neurodegeneration. *Transl. Vis. Sci. Technol.* **3**, 1 (2014).
54. J. D. Cahoy *et al*., A transcriptome database for astrocytes, neurons, and oligodendrocytes: A new resource for understanding brain development and function. *J. Neurosci.* **28**, 264–278 (2008).
55. H. L. Park, J. H. Kim, C. K. Park, Different contributions of autophagy to retinal ganglion cell death in the diabetic and glaucomatous retinas. *Sci. Rep.* **8**, 13321 (2018).
56. Y. Lee *et al*., Oligodendroglia metabolically support axons and contribute to neurodegeneration. *Nature* **487**, 443–448 (2012).
57. U. Fünfschilling *et al*., Glycolytic oligodendrocytes maintain myelin and long-term axonal integrity. *Nature* **485**, 517–521 (2012).
58. R. Bruzzone, C. Giaume, Connexins and information transfer through glia. *Adv. Exp. Med. Biol.* **468**, 321–337 (1999).
59. F. Fei, D. M. Bowdish, B. E. McCarry, Comprehensive and simultaneous coverage of lipid and polar metabolites for endogenous cellular metabolomics using HILIC-TOF-MS. *Anal. Bioanal. Chem.* **406**, 3723–3733 (2014).
60. A. Akopian *et al*., Targeting neuronal gap junctions in mouse retina offers neuroprotection in glaucoma. *J. Clin. Invest.* **127**, 2647–2661 (2017).
61. L. Xing, T. Yang, S. Cui, G. Chen, Connexin hemichannels in astrocytes: Role in CNS disorders. *Front. Mol. Neurosci.* **12**, 23 (2019).
62. T. D. Montero, J. A. Orellana, Hemichannels: New pathways for gliotransmitter release. *Neuroscience* **286**, 45–59 (2015).
63. J. Kang *et al*., Connexin 43 hemichannels are permeable to ATP. *J. Neurosci.* **28**, 4702–4711 (2008).
64. C. Meunier *et al*., Contribution of astroglial Cx43 hemichannels to the modulation of glutamatergic currents by D-serine in the mouse prefrontal cortex. *J. Neurosci.* **37**, 9064–9075 (2017).
65. N. Bazargani, D. Attwell, Astrocyte calcium signaling: The third wave. *Nat. Neurosci.* **19**, 182–189 (2016).
66. S. A. Liddelow *et al*., Neurotoxic reactive astrocytes are induced by activated microglia. *Nature* **541**, 481–487 (2017).
67. A. Bevilacqua, R. Loch-Caruso, R. P. Erickson, Abnormal development and dye coupling produced by antisense RNA to gap junction protein in mouse preimplantation embryos. *Proc. Natl. Acad. Sci. U.S.A.* **86**, 5444–5448 (1989).